Experimental Validation of a Real-Time Digital Twin for Latency and Performance Analysis in Automated Wood-Framing

Djamel Eddine Touil[1], Jordan Kolb[1], Ahmed Bouferguene[2], Yasser Mohamed[1], Mohamed Al-Hussein[1] and Simaan AbouRizk[1]

[1]Department of Civil & Environmental Engineering, University of Alberta, Edmonton, AB, T6G 1H9, Canada
[2]Campus Saint-Jean, University of Alberta, Edmonton, AB, T6C 3N2, Canada

touil@ualberta.ca

Abstract -

Digital twins (DTs) have become a cornerstone of cyber-physical systems, enabling real-time monitoring, control, and predictive analytics through continuous data exchange between physical assets and their virtual counterparts. While extensively applied in manufacturing, their adoption in off-site wood construction remains limited, particularly with respect to experimentally validated synchronization and latency analysis. This paper presents a real-time digital twin of a wood-framing machine that integrates the Robot Operating System (ROS), Gazebo simulation, and a Schneider M251 programmable logic controller (PLC) to achieve unified sensing, visualization, and control. The proposed framework reproduces the machine's kinematics, assembly operations, and control logic in a virtual environment while streaming encoder and force feedback for live condition monitoring. Experimental validation demonstrates sub-second synchronization, with average latencies of 0.39 s at the visualization level and 0.12 s at the control level. Machine-driven operations exhibit deviations below 3%, while human-dependent tasks remain within 10%. The proposed architecture delivers a validated real-time synchronization and predictive monitor-ing, providing a foundation for scalable automation in off-site construction.

Keywords -

Digital Twin; Wood Framing; Construction; Off-Site; BIM

1 Introduction

The digital twin (DT) concept, first articulated by Grieves in the early 2000s, describes a virtual counterpart of a physical product comprising three components: the physical asset, its digital representation, and their continuous bidirectional data exchange [1]. DTs have since become a key enabler of Industry 4.0, driven by advances in IoT, data analytics, and machine learning [2], with definitions from Siemens [3] and IBM [4] consistently aligned with this model. DTs merge physical and virtual environments through IoT integration and advanced analytics, enabling predictive maintenance, fault detection, and process optimization. Their closed-loop data exchange supports real-time decision-making and dynamic control, forming a "digital thread" that connects an asset's lifecycle and improves resource efficiency [5]. Applications now span manufacturing, automotive, aerospace, construction, and energy sectors [6]. In robotics, DTs integrated with MATLAB, Simulink, and ROS have optimized manipulator design and control [2], while cloud-based frameworks leveraging 5G and fog computing enable autonomous decision-making in smart factories [7]. In smart manufacturing, DTs support flexible production systems, real-time monitoring, and AI-driven optimization using genetic algorithms, deep learning, and reinforcement learning [8, 9]. Practical implementations include robotic arms [10], sensor-driven stress analysis [11], and condition-based robotic drilling [12]. Despite these advances, most DT frameworks remain limited to software-level simulations without empirical validation of real-time synchronization [4, 6, 7, 13, 14], with only limited hardware integration or quantitative fidelity assessment [2, 9, 12, 15]. Recent work by Hlayel et al. [5] benchmarked WebSocket, MQTT, Modbus, and OPC UA protocols for DT integration, demonstrating that WebSocket–S7 achieved 87 ms latency under IEC 61588 constraints. However, their analysis remained at the protocol level without system-level synchronization or closed-loop control validation. In off-site construction, DT applications remain restricted to simulation-based scheduling [3], lacking physical machine connectivity or validated timing performance. This study addresses these gaps by developing and experimentally validating a physically connected DT of a wood-framing machine (WFM) that: (i) establishes bidirectional synchronization between control and visualization layers, (ii) quantifies dual-layer latency against IEC 61588 and ISO 23247 standards, (iii) evaluates predictive fidelity for deterministic and human-dependent tasks, and (iv) integrates BIM-derived panel specifications as direct machine-level control inputs.

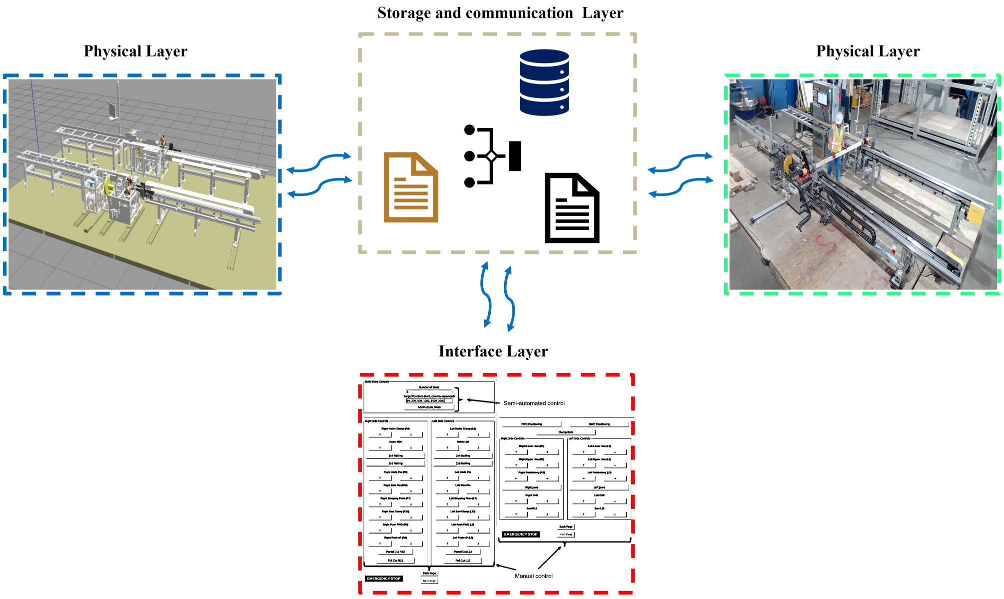

Figure 1. Four-layer WFM digital twin architecture.

2 Methodology

As illustrated in Fig. 1, the proposed DT framework adopts a four-layer architecture comprising: (1) the Physical Layer with PLC-controlled WFM hardware, (2) the Communication Layer utilizing Modbus TCP for real-time data exchange, (3) the Digital Layer integrating ROS Gazebo simulation and a Unified Robot Description Format (URDF) based machine model, and (4) the Interface Layer featuring a Python-based GUI for monitoring and control. Information flows cyclically between the physical WFM and its digital counterpart, where the PLC acquires sensor data and transmits it to the DT through Modbus TCP, while the ROS–Gazebo model visualizes and simulates operations in near real time. Control commands and feedback loops close the synchronization cycle, enabling unified data acquisition, analysis, and predictive visualization across the physical–digital system.

Table 1. Wood framing machine parameters

Station	**Joint**	**F/T**	**Vel.**
Drill	Vertical movement	433 N	1 m/s
	Horizontal movement	433 N	1 m/s
	Clamp	332 N	0.2 m/s
Cutting	Saw vertical movement	122 N	0.11 m/s
	Saw clamp	665 N	0.42 m/s
	Gripper joint	36.3 N	26.25 r/s
Nailing	Pin horizontal movement	609 N	0.38 m/s
	Pin vertical shaft	1623 N	1 m/s
	Stopping plate	1040 N	0.45 m/s
	Nailing clamp	1623 N	0.5 m/s
	Nailing clamp shaft	1040 N	1 m/s
	Nailer vertical movement	238 N	0.08 m/s
Positioning	Horizontal movement	1423 N	0.23 m/s
	Lower dragging jaw	866 N	1 m/s
	Upper dragging jaw	1040 N	1 m/s
Height Adj.	Horizontal movement	1018 N	0.21 m/s

2.1 Physical Layer

The automated WFM consists of four tool sections per side, covering an area of 33.7 m^2 and weighing 1022.6 kg. Force, torque, and deflection analyses validated the selection of motors and actuators, ensuring reliable motion for all framing operations. The machine's operational limits and joint parameters are summarized in Table 1.

The production sequence begins at the drilling station, featuring vertical and horizontal actuators with a pneumatic table clamp. The cutting station integrates a vertically driven saw and a gripper clamp for workpiece stabilization. The nailing station combines horizontal and vertical pneumatic cylinders with a 45° stopping plate and a vertically actuated electric nailer for fastening. Completed panels are transferred through an offloading station composed of conveyor tables and a servo-driven clamping-dragging jaw system, while the entire right-side assembly can be horizontally repositioned by a NEMA 34 ball-screw actuator to accommodate various panel sizes.

The physical WFM operates through industrial hardware controlled by a Schneider M251 PLC. The PLC manages all actuators and sensors using SoMachine 4.1 [16], ensuring coordinated motion across drilling, cutting, nailing, positioning, and conveying stations.

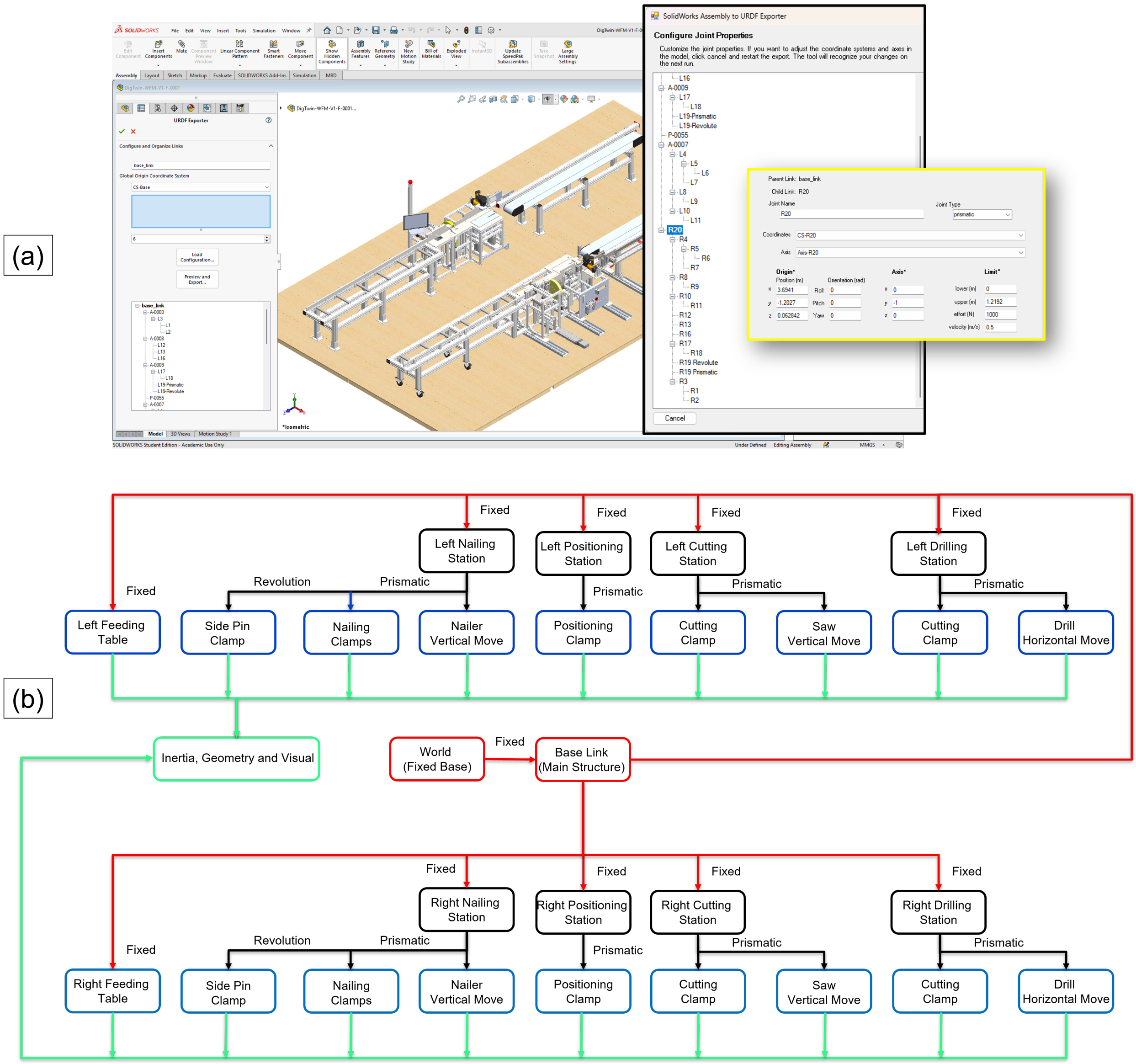

Figure 2. (a) SolidWorks assembly with URDF Exporter, (b) WFM hierarchical structure for ROS integration.

2.2 Digital Layer

The virtual representation of the WFM is derived from the SolidWorks assembly, which is exported to URDF format for integration with ROS and Gazebo. The model defines all joints, link dependencies, and station hierarchies required for simulation and visualization. Fig. 2a shows the SolidWorks assembly, while Fig. 2b illustrates the corresponding hierarchical structure used in the digital twin. Once exported, the URDF model is deployed in ROS, where Gazebo provides physics-based simulation when required. Python control scripts handle data exchange between the simulation and the real WFM, with the Joint State Publisher (JSP) generating joint states and the Robot State Publisher (RSP) publishing the associated 3D link poses. The Joint Trajectory Controller (JTC) is configured through the ROS launch file, which specifies controller parameters, joint assignments, and operational limits, and initializes both the RSP and the Gazebo environment while spawning the WFM model. A dedicated Python node drives the JTC by receiving user-defined joint inputs and forwarding them to the ROS–Gazebo plugin, ensuring consistent virtual behavior during simulation and visualization.

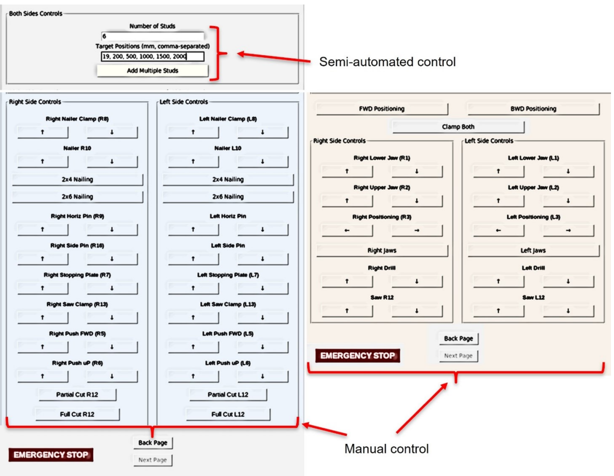

Figure 3. JSP GUI for manual and automated control of the WFM.

2.3 Interface Layer

The JSP graphical user interface (GUI), developed in Python, provides an interface for manually controlling the WFM joints, as shown in Fig. 3. Dedicated buttons for prismatic and revolute joints allow each component to be actuated independently, enabling operators to manipulate subsystems such as the nailer, saw, drill, clamps, pins, and positioning motors. This manual mode is valuable for testing, calibration, and demonstration purposes. In addition, the GUI supports automated operation by integrating with Building Information Modeling (BIM) data, extracting critical panel information such as stud count, spacing, and placement positions in millimeters, which are translated into machine-level instructions with minimal human intervention. For example, a panel specifying 7 studs at 406 mm spacing generates positioning commands at $x = 406, 812, 1218, \ldots$ mm, with the nailer executing a fixed 2-nail sequence per stud, eliminating manual parameter entry and reducing setup time.

2.4 Storage and Communication Layer

To enable simulation and control integration, ROS Noetic was installed on Ubuntu 20.04 within the Windows Subsystem for Linux (WSL). As illustrated in Fig. 4a, a seamless bridge was established between the physical WFM and its digital twin. Communication between the physical WFM and the digital twin is achieved via the PLC's networking capabilities, notably Modbus TCP, enabling synchronization between real-world operations and the virtual representation. In addition to real-time communication, all operational data such as sensor values, actuator states, and cycle-time logs were stored in the local database connected to the SCADA system. As depicted in Fig. 4b, a Python scripts using SQL queries were employed to retrieve these data records directly from the database for analysis, calibration, and validation of the digital twin. This integration of communication and storage layers ensured that both real-time and historical datasets were available for synchronization assessment and predictive modeling.

3 Results and Discussion

The proposed digital twin framework was implemented and executed on a workstation equipped with an Intel(R) Core(TM) Ultra 9 285K CPU running at 3.70 GHz, 128 GB RAM, and an NVIDIA RTX 4500 Ada Generation GPU with 24 GB of dedicated memory. This section is organized into two analytical subsections.

3.1 Synchronization Accuracy

The objective of this experiment was to assess the real-time congruence between the DT and the physical WFM, ensuring that the virtual model accurately mirrored the machine's operational behavior. The demonstration video available at `https://drive.google.com/file/d/1lTqKGhAauzvqK-xrtKiDugoKhPo1oT7S/view?usp=sharing` shows the DT executing at the positioning station, confirming that the simulated kinematics closely matched the physical motion.

Latency was evaluated at the visualization and control levels to characterize timing between the physical and digital systems. It originates from PLC scan cycles (20 ms), network communication, and computational overhead in the ROS–Gazebo environment, where physics calculations, joint-state updates (published at 50 Hz), and rendering tasks influence real-time performance.

Visualization latency was measured as the difference between synchronized Network Time Protocol (NTP) timestamps from the SCADA database and the ROS message headers, representing the delay between each PLC event and its corresponding update in the ROS–Gazebo interface (published at 50 Hz). Control latency was obtained from the round-trip delay between command transmission from the Schneider M251 PLC over Modbus TCP to the digital twin. Each measurement was repeated across multiple operations, and the mean, standard deviation, and maximum values were calculated to assess timing stability. The delay for each operation was computed as:

$$d_i = t_i^{DT} - t_i^{PHY}, \quad (1)$$

where t_i^{DT} and t_i^{PHY} represent the stamp times recorded by the digital twin and the physical machine, respectively. The mean delay μ_d, standard deviation σ_d, and maximum

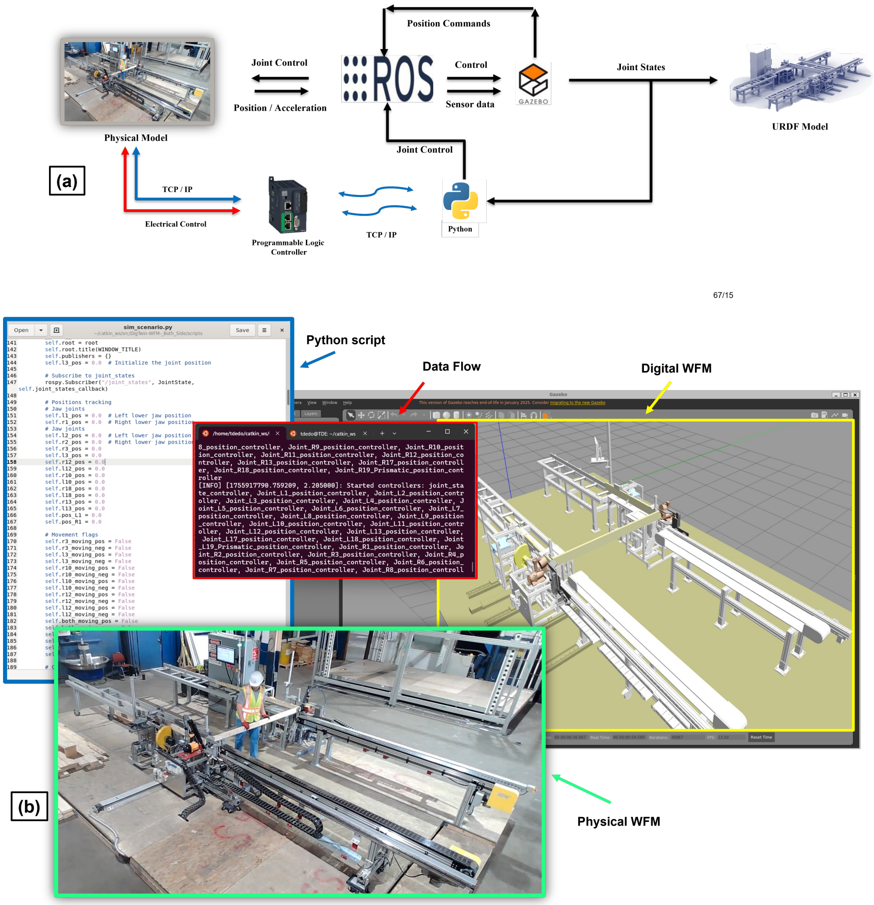

Figure 4. (a) WFM-digital twin communication framework via PLC and ROS-Gazebo. (b) Synchronized operations between digital and physical WFM.

delay d_{max} were determined using:

$$
\begin{aligned}
\mu_d &= \frac{1}{N} \sum_i d_i, \\
\sigma_d &= \sqrt{\frac{1}{N} \sum_i (d_i - \mu_d)^2}, \\
d_{max} &= \max_i d_i.
\end{aligned} \tag{2}
$$

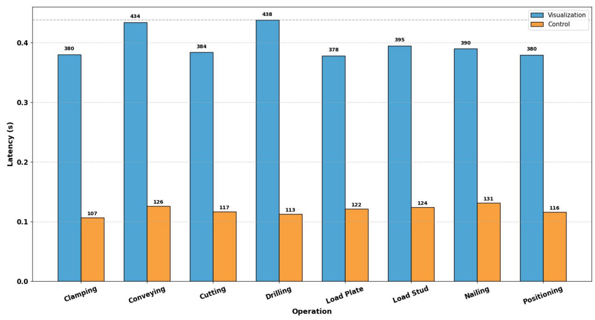

Figure 5. Visualization-layer synchronization latency between the physical WFM and digital twin.

Figs. 5 and 6 illustrate the synchronization performance at both visualization and control levels, with statistical indicators capturing both the mean delay and the variability in synchronization accuracy across five runs, thereby providing insight into overall system stability. The visualization latency exhibited mean delays between 0.38 s and 0.44 s, consistent with the 200–500 ms range typically reported for near real-time digital twin visualization in manufacturing systems [5]. The lowest mean latency was observed for clamping and positioning operations with 0.38 s, while the highest occurred during drilling and conveying with 0.44 s. Overall, the visualization latency maintained an average delay of $\mu_d = 0.390$ s with $\sigma_d = 0.036$ s and $d_{max} = 0.490$ s. These results demonstrate stable sub-second synchronization and confirm that the DT achieves reliable real-time correspondence suitable for supervisory visualization and process monitoring. In contrast, the control latency achieved substantially lower latency, with mean delays ranging from 0.106 s to 0.131 s and a maximum of 0.137 s. The overall average delay was $\mu_d = 0.120$ s, with $\sigma_d = 0.010$ s, satisfying the deterministic communication limits of 100–150 ms defined by IEC 61588 and ISO 23247 [5]. This represents approximately a fourfold improvement relative to the DT–PyhT visualization link, reflecting the reduced protocol overhead and direct register access characteristic of Modbus TCP communication.

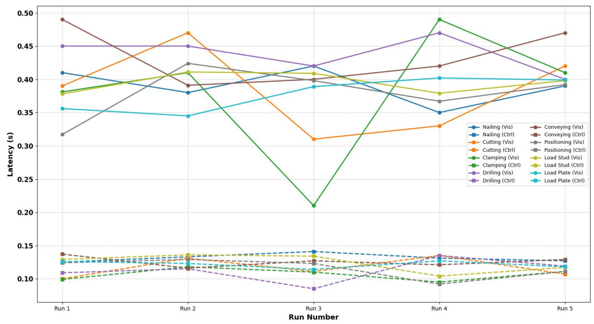

Figure 6. Control-level synchronization latency between the DT and the PLC.

The combined outcomes validate the synchronization strategy implemented within the proposed digital twin architecture. The upper visualization layer provides a delay-tolerant channel for high-fidelity monitoring and analytics, while the lower Modbus-based control layer ensures deterministic performance for real-time coordination.

3.2 Predictive Capability Assessment

The additional objective was to evaluate the digital twin's capability to anticipate machine performance using historical and real-time data. Historical cycle-time records for each machine station including nailing, drilling, cutting, positioning, and conveying were retrieved from the system's database storage and used to calibrate the digital twin, ensuring precise replication of station-specific dynamics. These operational datasets, presented in Fig. 7, formed the basis for accurately reproducing machine performance within the digital environment. Following calibration, the digital twin was tested to predict the production sequence of a selected wood panel. Input specifications, including panel geometry, stud configuration, and component placement, were extracted from the BIM model, shown in Fig. 8, and supplied to the DT GUI to execute a virtual simulation of the framing process without a live connection to the physical WFM.

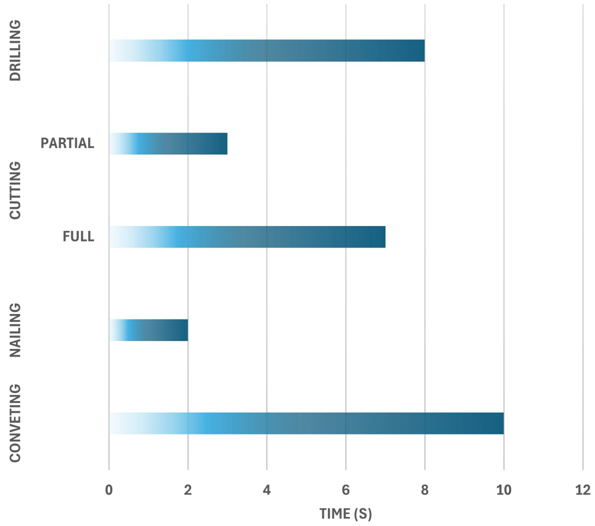

Figure 7. Historical WFM operation data.

The deviation between DT-predicted and Physical Twin (PhyT)-measured operation times was calculated using Eq. 3, where T_{DT} and T_{PhyT} represent the average durations obtained from the digital and physical systems, respectively. This quantitative comparison enables assessing how closely the digital twin replicates real machine performance across each operation.

$$\text{Deviation } (\%) = \frac{|T_{DT} - T_{PhyT}|}{T_{PhyT}} \times 100 \tag{3}$$

The results of the DT validation are presented in Figs. 9 and 10, comparing simulated operations against the corresponding Physical Twin (PhyT) processes on the WFM. In Fig. 9, the quantitative performance analysis demonstrates that most machine-controlled tasks, such as nailing, cutting, clamping, and conveyor transfer, show minimal deviation $\leq 3\%$, with calibration deviation of 2% also closely aligned and conveyor transfer achieving a perfect match of 1% deviation. These findings indicate that the DT accurately represents deterministic mechanical cycles. In con-

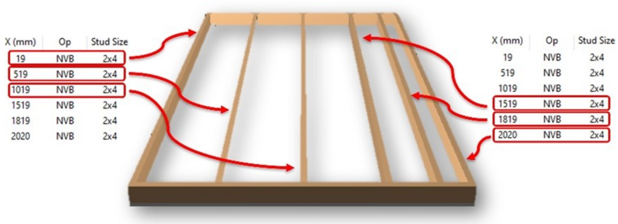

Figure 8. BIM of a wood panel with stud positions and sizes.

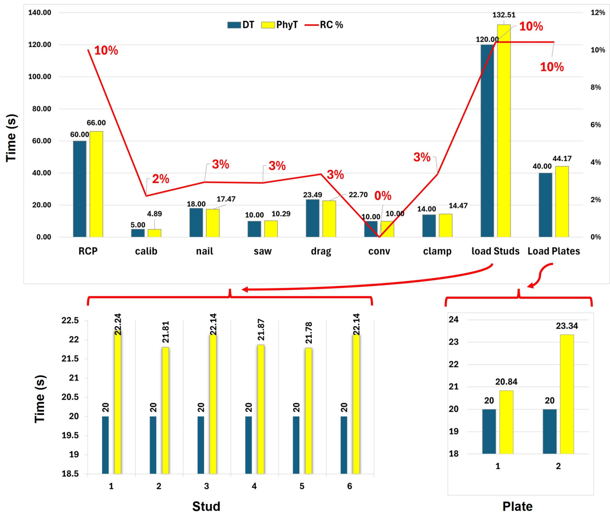

Figure 9. Comparison of DT-predicted and Physical-measured operation times for the WFM.

trast, handling-intensive operations, particularly stud and plate loading, exhibit higher deviations of approximately 10%, reflecting the influence of operator interaction, alignment adjustments, and material variability. The detailed breakdown confirms that the DT assumes constant deterministic times, whereas the PhyT introduces real times.

In Fig. 10, the process-level comparison between the DT simulation (top row) and the PhyT assembly process (bottom row) further supports these findings. Both follow the same operational order, from base plate positioning to the sequential addition of studs, resulting in equivalent final panel configurations. The DT successfully replicates the production logic and structural outcome, demonstrating its effectiveness in capturing workflow and assembly behavior. Minor discrepancies in timing and positioning in the physical process highlight real-world uncertainties not yet fully modeled in the DT, such as material imperfections, frictional resistance, and human-in-the-loop effects. Comparative analysis of the virtual and physical outcomes demonstrated that the DT can accurately forecast machine performance for the given production scenario, thereby confirming its effectiveness as a predictive and planning tool. These results demonstrate that the DT not only reproduces physical sequencing but also enables predictive estimation of process durations under varying configurations. This quantitative validation provides the foundation for extending the DT toward adaptive control and predictive scheduling of future production cycles.

While prior DT implementations in robotics and manufacturing validated virtual synchronization qualitatively [2, 12, 15], they did not systematically quantify real-time offset or predictive deviation. The present framework introduces a measurable fidelity analysis, correlating machine operation timestamps and digital synchronization to evaluate latency, deviation, and synchronization consistency. This quantitative comparison provides a new performance dimension for assessing DT reliability under real operational conditions.

4 Conclusion and Future Work

This study developed and validated a real-time digital twin (DT) of a wood-framing machine integrating ROS, Gazebo, and PLC-based sensing for synchronized monitoring and control. The DT achieved average latencies of 0.39 s at the visualization level and 0.12 s at the control level, meeting real-time operation requirements. Machine-driven tasks showed deviations below 3%, while human-influenced operations remained within 10%, demonstrating high predictive fidelity.

The current implementation was tested on a single workstation and one wall-panel configuration, limiting generalization across projects and operating conditions. Clock synchronization relied on NTP rather than PTP, and the simulation ran in open-loop mode without feedback control. Future work will extend testing to multiple panels and production scenarios, implement closed-loop control, and evaluate scalability and latency reduction for multi-machine integration in automated off-site construction. This validation bridges the gap between conceptual digital twins and practical deployment in automated off-site construction.

References

[1] M Grieves. Origins of the digital twin concept. florida institute of technology/nasa, 2016.

[2] Senthamarai Kannan Chinnasamy, Hari Prasaanth Sura, Amanullah Saleem, Akash Kathirvel, and Prashanna Rangan. Digital twin of robot manipulator using ros. In *AIP Conference Proceedings*, volume 2946, page 040004. AIP Publishing LLC, 2023.

[3] Fatima Alsakka, Haitao Yu, Ibrahim El-Chami, Farook Hamzeh, and Mohamed Al-Hussein. Digital twin for production estimation, scheduling and real-time monitoring in offsite construction. *Computers & Industrial Engineering*, 191:110173, 2024.

[4] Tho V Le and Ruoling Fan. Digital twins for logistics and supply chain systems: Literature review, conceptual framework, research potential, and practical challenges. *Computers & industrial engineering*, 187:109768, 2024.

[5] Mohammed Hlayel, Hairulnizam Mahdin, and Husaini Aza Mohd Adam. Latency analysis of

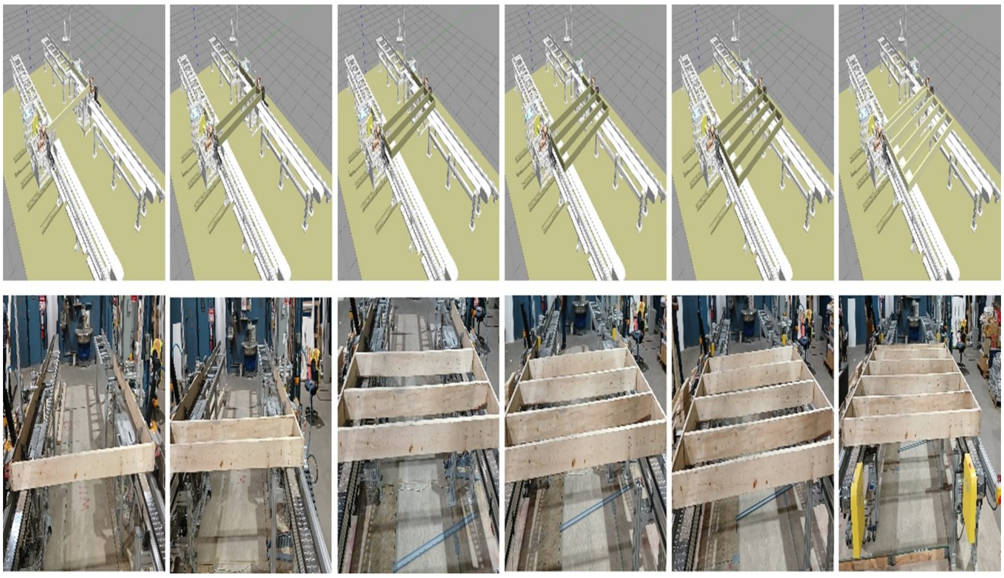

Figure 10. (Top) Stepwise panel assembly in the digital twin and (bottom) physical WFM.

websocket and industrial protocols in real-time digital twin integration. *International Journal of Engineering Trends and Technology*, 73(1): 120–135, 2025. doi:10.14445/22315381/IJETT-V73I1P110. URL `https://doi.org/10.14445/22315381/IJETT-V73I1P110`.

[6] Maulshree Singh, Rupal Srivastava, Evert Fuenmayor, Vladimir Kuts, Yuansong Qiao, Niall Murray, and Declan Devine. Applications of digital twin across industries: A review. *Applied Sciences*, 12 (11):5727, 2022.

[7] Hoa Tran-Dang and Dong-Seong Kim. Digital twin-empowered intelligent computation offloading for edge computing in the era of 5g and beyond: A state-of-the-art survey. *ICT Express*, 2025.

[8] Xin Liu, Du Jiang, Bo Tao, Guozhang Jiang, Ying Sun, Jianyi Kong, Xiliang Tong, Guojun Zhao, and Baojia Chen. Genetic algorithm-based trajectory optimization for digital twin robots. *Frontiers in Bioengineering and Biotechnology*, 9:793782, 2022.

[9] Yongkui Liu, He Xu, Ding Liu, and Lihui Wang. A digital twin-based sim-to-real transfer for deep reinforcement learning-enabled industrial robot grasping. *Robotics and Computer-Integrated Manufacturing*, 78:102365, 2022.

[10] Albert Tai, Michael Chun, Yuqiu Gan, Mert Selamet, and Hod Lipson. Para: A one-meter reach, two-kg payload, three-dof open source robotic arm with customizable end effector. *HardwareX*, 10:e00209, 2021.

[11] Fahmi Bellalouna. Case study for design optimization using the digital twin approach. *Procedia CIRP*, 100:595–600, 2021.

[12] Ahmad Farhadi, Stephen KH Lee, Eoin P Hinchy, Noel P O'Dowd, and Conor T McCarthy. The development of a digital twin framework for an industrial robotic drilling process. *Sensors*, 22(19):7232, 2022.

[13] Baicun Wang, Fei Tao, Xudong Fang, Chao Liu, Yufei Liu, and Theodor Freiheit. Smart manufacturing and intelligent manufacturing: A comparative review. *Engineering*, 7(6):738–757, 2021.

[14] Anjela Mayer, Lucas Greif, Tim Markus Häußermann, Simon Otto, Kevin Kastner, Sleiman El Bobbou, Jean-Rémy Chardonnet, Julian Reichwald, Jürgen Fleischer, and Jivka Ovtcharova. Digital twins, extended reality, and artificial intelligence in manufacturing reconfiguration: A systematic literature review. *Sustainability*, 17(5):2318, 2025.

[15] Francisco José Mañas-Álvarez, María Guinaldo, Raquel Dormido, and Sebastian Dormido-Canto. Scalability of cyber-physical systems with real and virtual robots in ros 2. *Sensors*, 23(13):6073, 2023.

[16] Fanel-Viorel Panaitescu, Mariana Panaitescu, and Daniela-Elena Juganaru. Monitoring and data acquisition for a consumption system based on renewable energies. *Int. Journal of Modern Manufacturing technologies*, 14(3):184–190.